Reciprocity of propagation in optical fiber links demonstrated to 10–21

Dan Xu, Pacôme Delva, Olivier Lopez, Anne Amy-Klein, Paul-Eric Pottie

Research Article | Vol. 27, No. 25 / 9 December 2019 / Optics Express 36965
Optics EXPRESS

Reciprocity of propagation in optical fiber links demonstrated to 10^{-21}

Dan Xu,[1] Pacôme Delva,[1] Olivier Lopez,[2] Anne Amy-Klein,[2] and Paul-Eric Pottie[1,*]

[1]LNE-SYRTE, Observatoire de Paris, Université PSL, CNRS, Sorbonne Université, 61 Avenue de l'Observatoire, 75014 Paris, France
[2]Laboratoire de Physique des Lasers, Université Paris 13, CNRS, 99 Avenue Jean-Baptiste Clément, 93430 Villetaneuse, France
*paul-eric.pottie@obspm.fr

Abstract: We present a study of the fundamental limit of fiber links using dedicated link architecture. We use an experimental arrangement that enables us to detect the forward and backward propagation noise independently and simultaneously in optical fiber and where the optical phase evolution is expected to be driven by the only contribution of the reference arms of the Michelson interferometer ensemble. In this article, we demonstrate indeed the high correlation between the optical phase evolution and the temperature variation of the interferometer ensemble, leading to a frequency offset of $(4.4 \pm 2.3) \times 10^{-21}$. Using a simple temperature model and a Bayesian analysis to evaluate the model parameters, we show that the temperature effect can be compensated with post-processing, removing the frequency offset down to $(0.5 \pm 2.0) \times 10^{-21}$. The residual slope of the optical phase evolution over 33 days is 350 yoctosecond/s. Using a global temperature parameter, we divide these 33 days dataset in four subsets and analyse their uncertainties. We show that they are self-consistent when the temperature is taken into account. This provides an alternative method to evaluate the accuracy of a fiber link, especially when the dataset includes large dead times. The result is finally interpreted as a test of the reciprocity of the propagation delay in an optical fiber. This unprecedented transfer capability could enable the comparisons of future optical clocks with expected performance at 10^{-20} level and open new possibilities for stringent tests of special and general relativity.

1. Introduction

Today the trapped ion or neutral lattice optical clocks have already demonstrated fs-level timing jitter, fractional accuracy as well as instability in the low 10^{-18} in several laboratories around the world [1–7]. The outstanding performance makes the optical clocks ideal tools for precision measurement and fundamental physics tests, such as general relativity, temporal variation of the fundamental constant, search for dark matter, chronometric geodesy, and gravitational waves [8–17].

Frequency transfer over optical fiber links has become the most accurate and stable method to ensure dissemination of optical frequencies and direct comparison of optical frequency standards [9,13,18–20]. In consideration of the state-of-the-art atomic frequency standards accuracy, hitherto the uncertainty contributions of optical fiber links must be assessed rigorously. Optical frequency transfer with uncertainty as low as a few 10^{-20} were reported with various experimental implementation [21,22]. For further improvement, the laser source as a dominant source of phase noise in the long-term was demonstrated experimentally [23]. When the laser source can be set in common mode, the biggest effect arises from the so-called interferometric noise [24]. The interferometric noise was experimentally observed and reported [25]. The necessary uncommon optical path and their relative fluctuations in optical interferometer ensemble are known also as the main limitation for multi-branch frequency combs [26,27].

#371530 https://doi.org/10.1364/OE.27.036965
Journal © 2019 Received 4 Jul 2019; revised 6 Oct 2019; accepted 12 Oct 2019; published 5 Dec 2019

Optics EXPRESS

In this Letter, we present the experimental work on a 2×43 km fiber link and the data acquired in the frame of campaign of optical clock comparison, carried out during about one month in June 2017, between the National Physical Laboratory (NPL) in UK, Système de Références Temps-Espace (SYRTE) in France and the Physikalisch-Technische Bundesanstalt (PTB) in Germany. We want to assess the link contribution to the accuracy of the campaign, and we need to handle irregular and non continuous data. We present the analysis of a 33-days dataset, with large dead-times, that we sub-divided in 4 subsets. We add a temperature measurement, acting on the reference arms of the Michelson interferometers. We show the evidence of the high correlation of the optical phase excursion with the temperature inside the interferometers using a simple setup. This allows us to compensate for the interferometric noise, for the first time to the best of our knowledge, using post-processing techniques. Finally we produce the evaluation of the instability and accuracy of such an optical frequency transfer. Our very long dataset and rigorous evaluation allows to set stringent limit on a possible violation of reciprocity of the propagation on an urban fiber link, to the low 10^{-21} level.

2. Experimental scheme

The experimental setup, based on a hybrid fiber link in an urban area, is illustrated in Fig. 1 and was reported previously in [23,25]. In summary, we start with an ultra-stable laser operating at 1.5 μm, with sub-Hz line-width. Its typical frequency drift of approximately 1 Hz/s, is actively removed by referencing its frequency to an H-maser using an optical frequency comb and an offset-phase locked laser. The hybrid fiber link consists of a 43 km fiber pair, using two noise compensation techniques for each fiber. Fiber 1 is actively compensated by using Doppler cancellation technique, and Fiber 2 is passively compensated by Two-Way (TW) method [21,28]. Here the remote laser source, to be injected into Fiber 2, consists of the ultra-stable laser transmitted to LPL through actively compensated Fiber 1. It is thus a "virtual" ultra-stable laser. For that purpose, two fiber optical couplers and two Faraday mirrors (FM) at the local site are used to build two strongly unbalanced Michelson interferometers. Three bi-directional erbium-doped fiber amplifier (bi-EDFA) are used to compensate the transmission loss of the ultra-stable laser. A polarization controller (PC) is used to optimize the amplitude of two-way beat notes (OWB and OWF, see below) detected on PD2. A partial Faraday mirror (p-FM) makes a perfect fiber-length match at the remote site [23]. The beat notes on PD1 and PD2 are separated by their corresponding frequencies, then filtered, tracked, simultaneously recorded by a dead-time free frequency counter operated in Π-type and Λ-type with 1 s gate time.

With such an arrangement of our setup, 4 synchronized beat notes (denoted as ANC, RT, OWB, OWF) can be measured simultaneously providing abundant information on the fiber noise and their correlations can be computed. The ANC (active-noise compensated) beat note signal is detected on PD1, which consists of half of the beat note signal between the round-trip laser signal in Fiber 1 (after partial reflection on the p-FM at LPL) and the local short reference arm (on top left of Fig. 1). It exhibits half of the round-trip noise on Fiber 1. The beat notes RT (round-trip), OWB (one-way backward) and OWF (one-way forward) are detected on PD2 at different frequencies. RT is the beat note signal between the round-trip laser signals on Fiber 2 and on local short arm (on bottom left of Fig. 1). OWB is the beat note signal between the backward virtual laser signal (propagating from LPL to SYRTE) and the ultrastable laser signal. OWF is the beat note signal between the forward laser signal (propagating from SYRTE to LPL) and the virtual laser signal. RT, OWB and OWF exhibit the round-trip, backward and forward propagation noise on Fiber 2, respectively. The frequency data recorded with the frequency counter are filtered in order to eliminate cycle slips and down-times of the active noise compensation or the laser source. Then, the phase evolution of the 4 beat notes are obtained from the frequency data with 1-s gate time and are converted into a time error. The noise floor of the system can be computed *in situ* by a linear combination of (OWB+OWF-RT)/2. It is free of

Optics EXPRESS

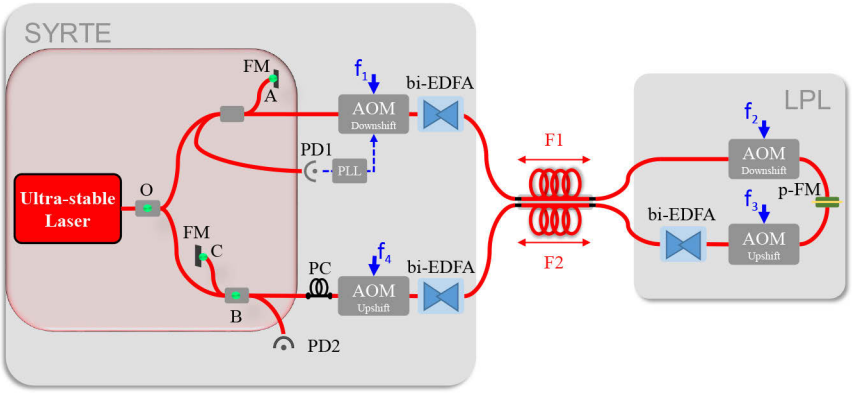

Fig. 1. Experimental scheme of the hybrid fiber link. AOM, acousto-optic modulator; PD, photodiode; PLL, phase-locked loop; bi-EDFA, bi-directional erbium-doped fiber amplifier; p-FM, partial Faraday mirror; PC, polarization controller. The laser and the interferometers are housed in a thermal and acoustic isolation box for passive stabilization.

the fiber noise (including temperature-induced noise) and thus corresponds to the detection noise floor. Additionally, it allows us also to check the reciprocity of the accumulated noise forth and back over a bi-directional fiber. Many technical details and experimental results are reported in [25]. In the experiment discussed here, we focus on the phase evolution of two-way bi-directional (TWB) observable, obtained by combining the forward and backward beat notes (OWB-OWF)/2.

In this setup, we take advantage of the optical frequency transfer made on the first fiber to eliminate the contribution to phase instability arising from the ultra-stable laser [23]. Then we are in a situation where the dominant noise source arises from the length mismatch between the two paths and the two reference arms of the fiber-based Michelson interferometers used for the optical phase detection at the local site [25]. This noise is referred to as interferometric noise [24,29]. We add a thermal sensor (10kOhms thermistor) inside the interferometer ensemble (the light red box shown in Fig. 1). A data logger is used to acquire the temperature data simultaneously. We look at the optical phase evolution of the two-way measurement and the expected phase evolution due to the temperature.

3. Experimental results

Figure 2 shows the optical phase evolution of TWB observable for 33 continuous days of operation of the fiber link. It is noticeable that a long interruption occurred at modified Julian data MJD = 57909 and 57910 due to an interruption of the ultra-stable light (no input signals). Except for that, the uptime over 31 days is estimated conservatively to 92%. To the best of our knowledge, this is the longest optical phase dataset reported so far. Moreover, real-time sensing and a fs-level tracking capability of the fiber induced phase noise are realized using our hybrid setup. It is noteworthy that the total phase evolution is just at the level of ~20 fs in the long-term. Thanks to the highly smooth phase evolution, significant diurnal fluctuation of $\phi_{\mathrm{TWB}}(t)$ is clearly visible over the timescale of 33 days continuous measurement. This periodic perturbation is also clearly seen on the power spectrum density (PSD) of fractional frequency as a peak at Fourier frequency of 1 day^{-1}, shown in Fig. 3.

The dominant noise source for the TWB observable is the interferometric noise. We found that the interferometric noise is mainly due to temperature variation on the optical length difference between the segments OA, OB and BC (see [25] for details and Fig. 1 for the definition of point O, A, B and C). The temperature variation inside the interferometer box is about 5 K over 33 days, and the daily variation is about 0.1 to 0.5 K. We apply the parameters of phase-temperature

Optics EXPRESS

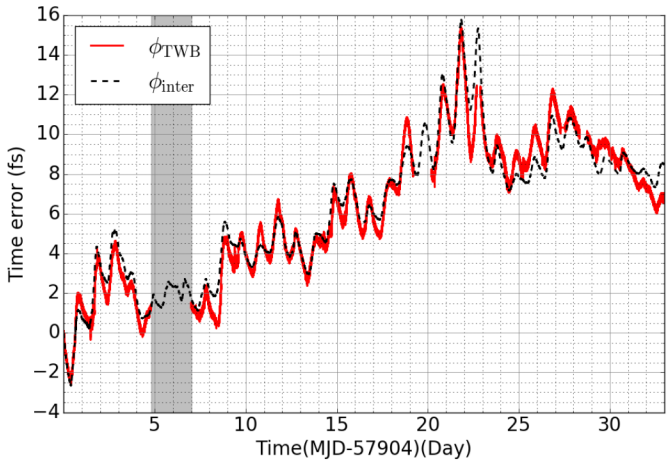

Fig. 2. Phase evolution of the two-way bi-directional (TWB) observable ϕ_{TWB} (red solid line) and interferometric noise ϕ_{Inter} (black dashed line), with 1-s gate time.

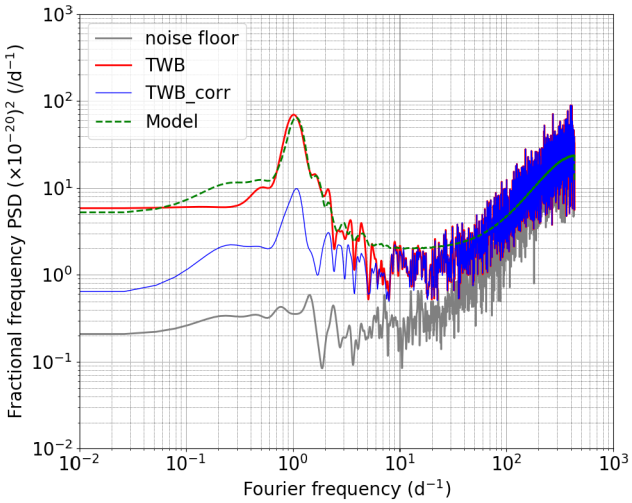

Fig. 3. Power spectral densities (PSD) of fractional frequency for noise floor (gray), the bi-directional two-way observable y_{TWB} (red), the model (green) and residuals after correction $y_{\mathrm{TWB\_corr}}$ (blue).

coefficient of silica fiber $\gamma \approx 37$ fsK^{-1}m^{-1}, and the length mismatch $\Delta L = L_{\mathrm{BC}} + L_{\mathrm{OA}} - L_{\mathrm{OB}} \approx 15$ cm [23], then obtain roughly the interferometric noise $\phi_{\mathrm{inter}}(t) = \gamma \Delta L \Delta T$, shown in Fig. 2 (black dashed line). Similar diurnal fluctuation for interferometric noise is observed over 33 days. The correlations between $\phi_{\mathrm{TWB}}(t)$ and $\phi_{\mathrm{inter}}(t)$ are evaluated at the high level of 97.6%. Intuitively, the effect of temperature variation on the optical phase evolution of $\phi_{\mathrm{TWB}}(t)$ is evident.

Before processing the data, we remove the fractional frequency data $y_{\mathrm{TWB}}(t)$ where the phase difference between another two TWB observables (combinations of round-trip and forward beat notes, round-trip and backward beat notes, see details in [25]) is more than 2 fs. After this second filtering stage, we keep around 80 % of data of the total measurement time. Taking care of discontinuities (more than 6 h) after data removal, the whole dataset is divided into 4 subsets. Before any further data processing, we also face the problem of running time for the 33 days' dataset computing. Therefore, we average the frequency data in groups of 100 in order to

Optics EXPRESS

estimate the model parameters, as displayed in Fig. 4(a). We have verified that this filtering does not change the results of the analysis.

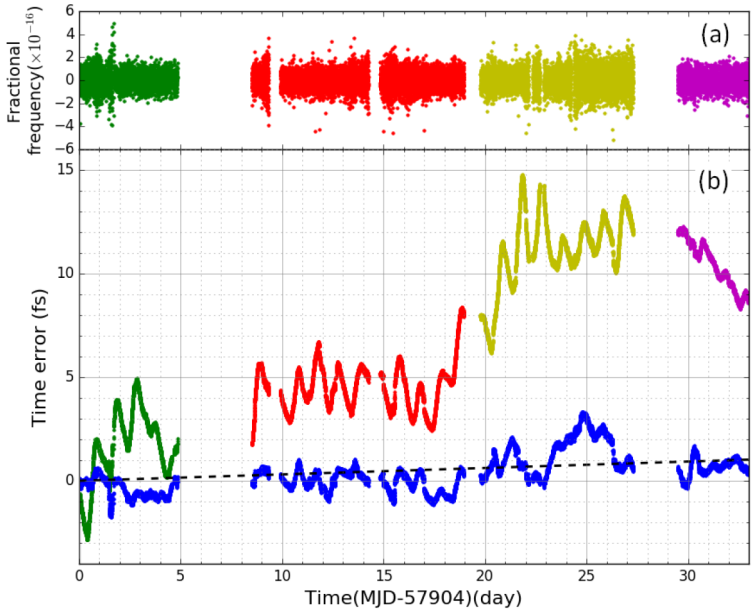

Fig. 4. Four data subsets. (a) Filtered fractional frequency, (b) phase evolution of TWB without temperature correction and with temperature correction (blue).

We use a simple model of the effect of temperature on the fractional frequency of the TWB observable, written as:

$$y_{\mathrm{TWB}}(t) = y_T + \mu_i + \epsilon \tag{1}$$

where y_T is the temperature-induced noise, μ_i ($i = 1, \ldots, 4$) is a constant (fractional frequency offset) for each data subset, and ϵ is the colored noise. The colored noise is modeled as a sum of white noise (PSD $\propto f^0$) with level σ_{WN} and violet noise (PSD $\propto f^2$) with level σ_{VN}, which is equivalent to white frequency noise plus white phase noise. This model is motivated by the characteristics of the noise floor PSD (see Fig. 3).

In the reference arm the propagation delay fluctuations are not simply proportional to temperature fluctuations and can be expanded as a function of successive derivatives of temperature, accounting for faster and faster temperature dependence. We have thus compared 4 different parametric models for the temperature-induced noise y_T, including the effect of the first-order and second-order derivative of the temperature, and the time delay between a temperature variation and its effect on the fractional frequency. The comparison shows that taking the second-order derivative of temperature or the delay into account does not change the results significantly, and can even lead to high correlations between model parameters when both the second-order derivative of temperature and the delay are estimated in the model. Therefore, the Bayesian analysis favors the simplest model as a consequence of Occam's razor [31]; it can be written as:

$$y_T = \alpha_T \frac{dT}{dt} \tag{2}$$

where dT/dt is the temperature variation, α_T is the frequency-temperature coefficient of silica fiber. We use the affine invariant ensemble Markov Chain Monte Carlo (MCMC) method for the fitting procedure [30]. We fit the TWB observable assuming flat priors on all parameters

Optics EXPRESS

except a Gaussian prior on the violet noise level σ_{VN}, which is formerly fitted on the noise floor observable which is free of temperature-induced noise. Indeed, it can be shown that the violet noise level σ_{VN} is similar on the TWB and the noise floor observables.

First we fit a model without temperature-induced noise: $y_{\mathrm{TWB\text{-}noTemp}}(t) = \mu_i + \epsilon$. The fitted set of parameters are $(\mu_i, \sigma_{\mathrm{WN}}, \sigma_{\mathrm{VN}})$ and results are given in Table 1. A frequency offset between 1-σ and 2-σ can be observed for all subsets. This is interpreted as an offset due to temperature which is not taken into account in the model.

Table 1. Fitting results using the affine invariant Markov Chain Monte Carlo ensemble sampler (MCMC) method. All parameters are dimensionless except for α_T in d·K^{-1}.

	Without y_T	With y_T
μ_1	$(5.26 \pm 5.34) \times 10^{-21}$	$(3.71 \pm 4.80) \times 10^{-21}$
μ_2	$(7.60 \pm 3.75) \times 10^{-21}$	$(2.03 \pm 3.13) \times 10^{-21}$
μ_3	$(6.66 \pm 4.42) \times 10^{-21}$	$(3.00 \pm 3.94) \times 10^{-21}$
μ_4	$(-11.32 \pm 6.46) \times 10^{-21}$	$(-11.37 \pm 5.07) \times 10^{-21}$
σ_{WN}	$(3.44 \pm 0.04) \times 10^{-19}$	$(2.90 \pm 0.04) \times 10^{-19}$
σ_{VN}	$(4.74 \pm 0.02) \times 10^{-19}$	$(4.83 \pm 0.02) \times 10^{-19}$
α_T	-	$(5.36 \pm 0.16) \times 10^{-20}$

Then, we fit the model given in Eq. (2), which takes into account the temperature effect. The fitted set of parameters is $(\mu_i, \sigma_{\mathrm{WN}}, \sigma_{\mathrm{VN}}, \alpha_T)$ and results are given in Table 1. The distributions of parameters are shown in Fig. 5. Only the μ_1 constant is presented in this figure for the sake of clarity; μ_2, μ_3, μ_4 have similar correlations with other parameters. The correlation coefficient between σ_{WN} and σ_{VN} is 0.32, while all other correlation coefficients are ~ 0.1 or below. The value of the temperature coefficient is $\alpha_T = (5.36 \pm 0.16) \times 10^{-20}$ d.K^{-1}, showing a very significant effect of temperature at more than 30-σ. Assuming a temperature coefficient of 37 fs/K/m we deduce a length mismatch of 13 cm, smaller than the previous measured one of 15cm [23]. The residual frequency $y_{\mathrm{TWB\_corr}}$ is integrated to obtain the corrected TWB phase $\phi_{\mathrm{TWB\_corr}}$, which is shown in Fig. 4(b). The corrected phase evolution is compatible with zero and is ranging in ±3 fs. The residual slope over the 33 days of integration is as low as 3.5×10^{-22} s/s (see the black dashed line in Fig. 4(b)).

The PSDs of the fitted model, TWB observable y_{TWB} and residual frequency $y_{\mathrm{TWB\_corr}}$ are shown in Fig. 3. The PSD of y_{TWB} behaves as white noise ($\propto f^0$) for frequencies $f \lesssim 0.3$ d^{-1}, shows a significant peak at 1 d^{-1} due to the diurnal temperature fluctuations of the interferometers, and behaves as violet noise ($\propto f^2$, equivalent to white phase noise) for $f \gtrsim 200$ d^{-1}. The PSD of $y_{\mathrm{TWB\_corr}}$ shows similar behavior as y_{TWB} but with obvious phase noise compression and the value of the peaks at Fourier frequency of 1 d^{-1} is reduced by a factor of 7.

The modified Allan deviation (MDEV) of the one-way observable, TWB observable y_{TWB} and residual frequency $y_{\mathrm{TWB\_corr}}$ are shown in Fig. 6. The MDEV of y_{TWB} is 3.9×10^{-17} at integration time $\tau = 1$ s and decreases to 8.0×10^{-21} at $\tau = 400\,000$ s. The stability curve shows a bump for 10 000 s $< \tau <$ 40 000 s, which is explained by the diurnal temperature fluctuation of the local interferometers. The MDEV of $y_{\mathrm{TWB\_corr}}$ shows no difference for $\tau \lesssim 1000$ s, but shows a great improvement after $\tau \sim 1000$ s. The diurnal bump is almost suppressed and the MDEV decreases to 3.0×10^{-21} at $\tau = 400\,000$ s, showing an improvement with a factor ~ 2.7.

To assess the accuracy contribution of the fiber link during a clock comparison campaign, we face the difficulty of handling with irregular and non continuous data with gaps [32]. Here we follow a rigorous method based on the noise model fitting. Table 1 reports for the frequency offsets μ_i obtained from the fit with and without temperature-induced noise model for each of the 4 subsets of data. The uncertainty of each subset was evaluated from the fitting procedures taking violet noise and white noise into account. We find out that without compensation the

Optics EXPRESS

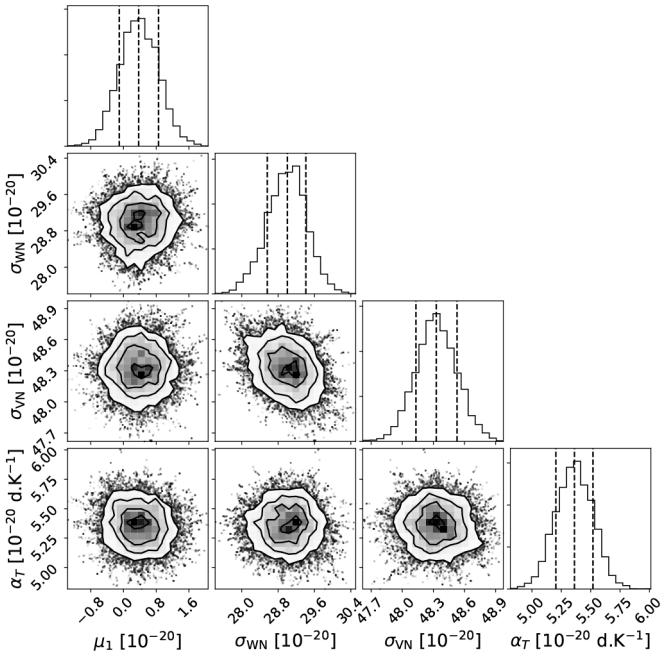

Fig. 5. One- and two-dimensional projections of posterior distribution of the estimated model parameters with 1-, 2- and 3-σ contours, corresponding to the fit of the two-way bi-directional (TWB) frequency data, using affine invariant ensemble Markov Chain Monte Carlo (MCMC) method [30].

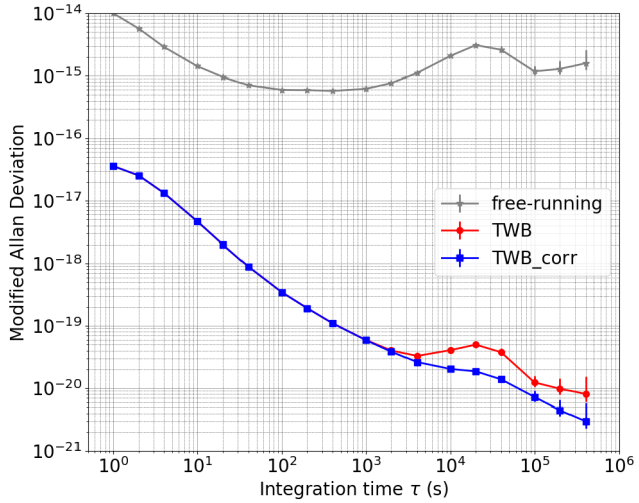

Fig. 6. Modified Allan deviation (MDEV) of the bi-directional two-way observable, before post-processing (red circle) and after post-processing (blue square), and one-way free-running fiber noise (gray star).

Optics EXPRESS

weighted mean and uncertainty of the offsets is $(4.4 \pm 2.3) \times 10^{-21}$, which is shown in Fig. 7(a) as a gray shaded area. When using the temperature model almost all frequency offsets are compatible within 1-σ, except μ_4 for the last subset. As shown in Fig. 7(b), the weighted mean and uncertainty of the offsets decrease down to $(0.5 \pm 2.0) \times 10^{-21}$. This gives an estimation of the accuracy of the optical link. For the last subset, the temperature model does not explain the fitted frequency offset. Indeed, it can be seen in Fig. 2 that the temperature is not well correlated to the optical phase evolution for the last 4 days of data. For the time being the effect cannot be related to another external phenomena, and we believe that this unexplained frequency offset should be related to another technical issues, that needs further investigation and would be the object of future work.

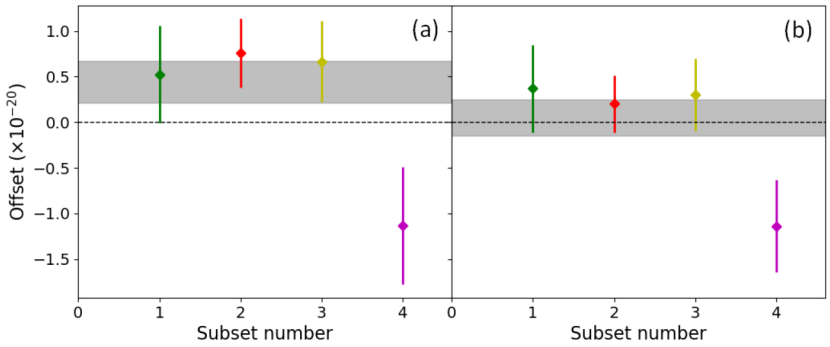

Fig. 7. The four subsets frequency offsets μ_i from Table 1 are shown with colors corresponding to Fig. 4. The grey thick line is centered on the μ_i weighted average with thickness corresponding to the weighted uncertainty. (a) Without temperature model, (b) with temperature model.

Finally the resulting uncertainty of the TWB observable can be interpreted as a test of propagation's reciprocity within an optical fiber. Indeed, using our hybrid set-up, we are in a particular situation where the laser phase difference and other technical issues related to geographical separation, such as common RF signal and acquisition de-synchronization, are not present. The mean value of the TWB observable represents a limit on potential frequency shift that may occur between two optical signal propagating with opposite direction in the same fiber [25]. Compared to our previous work [25], we can now set a limit as stringent as $(0.5 \pm 2.0) \times 10^{-21}$ for realistic in-field deployed single mode fiber in a urban area.

4. Conclusion

Using a simple temperature sensor and a Bayesian post-processing method we show unprecedented stability and accuracy for an optical frequency comparison, using an hybrid fiber link (transfer+comparison) between SYRTE and LPL. We demonstrate an effective correction of the interferometric noise, progressing towards extremely accurate remote frequency comparisons. We apply a alternative rigorous methodology to assess the accuracy of a coherent fiber link in the case where the dataset presents gaps or long periods of missing data. This methodology requires elaborate post-processing, but this is not a disadvantage in the case of extremely accurate clock comparisons.

The method introduced here permits to have an individual assessment of subset uncertainty, and to check the consistency of each dataset with the global uncertainty. In our case it permitted to isolate a subset where the frequency offset could not be explained with the simple temperature model, while a global analysis would not have permitted this discovery.

Optics EXPRESS

The current limitation of our results arises from the rare cycle slips, an issue that was so far little explored in the frame of satellite techniques [32,33], and still an open question for fiber links. In our setup, we have not yet implemented cycle slip detection techniques as done in the repeater laser station hardware implemented for long-haul cascaded fiber links. These supplementary data could help to safely remove outliers and improve the quality of the dataset [34,35]. We believe we can further improve the up-time and reach even longer integration time.

By the simplicity of the approach and the low-cost of its implementation, our methodology of temperature effect removal can be applied for a variety of optical systems using fiber-based interferometer ensemble, as for instance short fiber link linking two experiments or multi-branch optical frequency comb [26,27]. This work opens the way to simpler optical design, as the constraint on the interferometer optical path imbalance can be a little bit relaxed. It can be noticed that an active temperature stabilization could be implemented, but with the price of a greater complexity and risk of failure.

It is to be noticed that the hybrid scheme we presented here requires a net optical attenuation to be kept at the level of about 20 dB. This is therefore suitable for fiber links with a range of less than about 100 km, and could enable future comparison of optical clock using Fermi gases with expected accuracy of 10^{-20} level and open the way for the stringent tests of special and general relativity [5,36], as for example for test of Lorentz Invariance [9]. The extension of this work to long-haul links may not be straightforward, but we believe this type of architecture suits well for urban area with high density of optical clocks and can find immediate applications.

Funding

Agence Nationale de la Recherche (ANR-10-LABX-48-01, ANR-11-EQPX-0039); Institut National des Sciences de l'Univers, Centre National de la Recherche Scientifique (Action spécifique GRAM); European Association of National Metrology Institutes (15SIB05 (OFTEN), SIB-02 (NEAT-FT)).

Acknowledgments

We acknowledge funding support from the Agence Nationale de la Recherche (Labex First-TF ANR-10-LABX-48-01, Equipex REFIMEVE+ANR-11-EQPX-0039), Conseil Régional Ile-de-France (DIM Nano'K), CNRS with Action Spécifique GRAM, the European Metrology Research Programme (EMRP) in the Joint Research Projects SIB02 (NEAT-FT) and the European Metrology Programme for Innovation and Research (EMPIR) in project 15SIB05 (OFTEN). The EMRP and EMPIR are jointly funded by the EMRP/EMPIR participating countries within EURAMET and the European Union.

References

1. N. Huntemann, C. Sanner, B. Lipphardt, C. Tamm, and E. Peik, "Single-Ion Atomic Clock with 3×10^{-18} Systematic Uncertainty," Phys. Rev. Lett. **116**(6), 063001 (2016).
2. S. Origlia, M. S. Pramod, S. Schiller, Y. Singh, K. Bongs, R. Schwarz, A. Al-Masoudi, S. Dörscher, S. Herbers, S. Häfner, U. Sterr, and C. Lisdat, "Towards an optical clock for space: Compact, high-performance optical lattice clock based on bosonic atoms," Phys. Rev. A **98**(5), 053443 (2018).
3. N. Nemitz, T. Ohkubo, M. Takamoto, I. Ushijima, M. Das, N. Ohmae, and H. Katori, "Frequency ratio of Yb and Sr clocks with 5×10^{-17} uncertainty at 150 seconds averaging time," Nat. Photonics **10**(4), 258–261 (2016).
4. M. Schioppo, R. C. Brown, W. F. McGrew, N. Hinkley, R. J. Fasano, K. Beloy, T. H. Yoon, G. Milani, D. Nicolodi, J. A. Sherman, N. B. Phillips, C. W. Oates, and A. D. Ludlow, "Ultrastable optical clock with two cold-atom ensembles," Nat. Photonics **11**(1), 48–52 (2017).
5. S. L. Campbell, R. B. Hutson, G. E. Marti, A. Goban, N. Darkwah Oppong, R. L. McNally, L. Sonderhouse, J. M. Robinson, W. Zhang, B. J. Bloom, and J. Ye, "A Fermi-degenerate three-dimensional optical lattice clock," Science **358**(6359), 90–94 (2017).
6. G. E. Marti, R. B. Hutson, A. Goban, S. L. Campbell, N. Poli, and J. Ye, "Imaging Optical Frequencies with 100 μHz Precision and 1.1 μm Resolution," Phys. Rev. Lett. **120**(10), 103201 (2018).

Optics EXPRESS

7. M. S. Safronova, S. G. Porsev, C. Sanner, and J. Ye, "Two Clock Transitions in Neutral Yb for the Highest Sensitivity to Variations of the Fine-Structure Constant," Phys. Rev. Lett. **120**(17), 173001 (2018).
8. C. W. Chou, D. B. Hume, T. Rosenband, and D. J. Wineland, "Optical Clocks and Relativity," Science **329**(5999), 1630–1633 (2010).
9. P. Delva, J. Lodewyck, S. Bilicki, E. Bookjans, G. Vallet, R. Le Targat, P.-E. Pottie, C. Guerlin, F. Meynadier, C. Le Poncin-Lafitte, O. Lopez, A. Amy-Klein, W.-K. Lee, N. Quintin, C. Lisdat, A. Al-Masoudi, S. Dörscher, C. Grebing, G. Grosche, A. Kuhl, S. Raupach, U. Sterr, I. Hill, R. Hobson, W. Bowden, J. Kronjäger, G. Marra, A. Rolland, F. Baynes, H. Margolis, and P. Gill, "Test of Special Relativity Using a Fiber Network of Optical Clocks," Phys. Rev. Lett. **118**(22), 221102 (2017).
10. A. D. Ludlow, M. M. Boyd, J. Ye, E. Peik, and P. Schmidt, "Optical atomic clocks," Rev. Mod. Phys. **87**(2), 637–701 (2015).
11. A. Hees, J. Guéna, M. Abgrall, S. Bize, and P. Wolf, "Searching for an Oscillating Massive Scalar Field as a Dark Matter Candidate Using Atomic Hyperfine Frequency Comparisons," Phys. Rev. Lett. **117**(6), 061301 (2016).
12. Y. Stadnik and V. Flambaum, "Can Dark Matter Induce Cosmological Evolution of the Fundamental Constants of Nature?" Phys. Rev. Lett. **115**(20), 201301 (2015).
13. T. Takano, M. Takamoto, I. Ushijima, N. Ohmae, T. Akatsuka, A. Yamaguchi, Y. Kuroishi, H. Munekane, B. Miyahara, and H. Katori, "Geopotential measurements with synchronously linked optical lattice clocks," Nat. Photonics **10**(10), 662–666 (2016).
14. G. Lion, I. Panet, P. Wolf, C. Guerlin, S. Bize, and P. Delva, "Determination of a high spatial resolution geopotential model using atomic clock comparisons," J. Geod. **91**(6), 597–611 (2017).
15. S. Kolkowitz, I. Pikovski, N. Langellier, M. Lukin, R. Walsworth, and J. Ye, "Gravitational wave detection with optical lattice atomic clocks," Phys. Rev. D **94**(12), 124043 (2016).
16. P. Delva, H. Denker, and G. Lion, "Chronometric geodesy: Methods and applications," in *Relativistic Geodesy*, (Springer, 2019).
17. H. Denker, L. Timmen, C. Voigt, S. Weyers, E. Peik, H. S. Margolis, P. Delva, P. Wolf, and G. Petit, "Geodetic methods to determine the relativistic redshift at the level of 10^{-18} in the context of international timescales: a review and practical results," J. Geod. **92**(5), 487–516 (2018).
18. A. D. Ludlow, T. Zelevinsky, G. K. Campbell, S. Blatt, M. M. Boyd, M. H. G. de Miranda, M. J. Martin, J. W. Thomsen, S. M. Foreman, J. Ye, T. M. Fortier, J. E. Stalnaker, S. A. Diddams, Y. Le Coq, Z. W. Barber, N. Poli, N. D. Lemke, K. M. Beck, and C. W. Oates, "Sr Lattice Clock at 1×10^{-16} Fractional Uncertainty by Remote Optical Evaluation with a Ca Clock," Science **319**(5871), 1805–1808 (2008).
19. A. Yamaguchi, M. Fujieda, M. Kumagai, H. Hachisu, S. Nagano, Y. Li, T. Ido, T. Takano, M. Takamoto, and H. Katori, "Direct Comparison of Distant Optical Lattice Clocks at the 10^{-16} Uncertainty," Appl. Phys. Express **4**(8), 082203 (2011).
20. C. Lisdat, G. Grosche, N. Quintin, C. Shi, S. Raupach, C. Grebing, D. Nicolodi, F. Stefani, A. Al-Masoudi, S. Dörscher, S. Häfner, J.-L. Robyr, N. Chiodo, S. Bilicki, E. Bookjans, A. Koczwara, S. Koke, A. Kuhl, F. Wiotte, F. Meynadier, E. Camisard, M. Abgrall, M. Lours, T. Legero, H. Schnatz, U. Sterr, H. Denker, C. Chardonnet, Y. Le Coq, G. Santarelli, A. Amy-Klein, R. Le Targat, J. Lodewyck, O. Lopez, and P.-E. Pottie, "A clock network for geodesy and fundamental science," Nat. Commun. **7**(1), 12443 (2016).
21. A. Bercy, F. Stefani, O. Lopez, C. Chardonnet, P.-E. Pottie, and A. Amy-Klein, "Two-way optical frequency comparisons at 5×10^{-21} relative stability over 100-km telecommunication network fibers," Phys. Rev. A **90**(6), 061802 (2014).
22. S. M. F. Raupach, A. Koczwara, and G. Grosche, "Brillouin amplification supports 1×10^{-20} uncertainty in optical frequency transfer over 1400 km of underground fiber," Phys. Rev. A **92**(2), 021801 (2015).
23. W.-K. Lee, F. Stefani, A. Bercy, O. Lopez, A. Amy-Klein, and P.-E. Pottie, "Hybrid fiber links for accurate optical frequency comparison," Appl. Phys. B: Lasers Opt. **123**(5), 161 (2017).
24. P. A. Williams, W. C. Swann, and N. R. Newbury, "High-stability transfer of an optical frequency over long fiber-optic links," J. Opt. Soc. Am. B **25**(8), 1284–1293 (2008).
25. D. Xu, W.-K. Lee, F. Stefani, O. Lopez, A. Amy-Klein, and P.-E. Pottie, "Studying the fundamental limit of optical fiber links to the 10^{-21} level," Opt. Express **26**(8), 9515–9527 (2018).
26. K. Kashiwagi, Y. Nakajima, M. Wada, S. Okubo, and H. Inaba, "Multi-branch fiber comb with relative frequency uncertainty at 10^{-20} using fiber noise difference cancellation," Opt. Express **26**(7), 8831–8840 (2018).
27. A. Rolland, P. Li, N. Kuse, J. Jiang, M. Cassinerio, C. Langrock, and M. E. Fermann, "Ultra-broadband dual-branch optical frequency comb with 10^{-18} instability," Optica **5**(9), 1070–1077 (2018).
28. C. E. Calosso, E. Bertacco, D. Calonico, C. Clivati, G. A. Costanzo, M. Frittelli, F. Levi, A. Mura, and A. Godone, "Frequency transfer via a two-way optical phase comparison on a multiplexed fiber network," Opt. Lett. **39**(5), 1177–1180 (2014).
29. F. Stefani, O. Lopez, A. Bercy, W.-K. Lee, C. Chardonnet, G. Santarelli, P.-E. Pottie, and A. Amy-Klein, "Tackling the limits of optical fiber links," J. Opt. Soc. Am. B **32**(5), 787–797 (2015).
30. J. Goodman and J. Weare, "Ensemble samplers with affine invariance," Commun. Appl. Math. Comput. Sci. **5**(1), 65–80 (2010).
31. P. Gregory, *Bayesian Logical Data Analysis for the Physical Sciences* (Cambridge University, 2010).

Optics EXPRESS

32. I. Sesia, E. Cantoni, A. Cernigliaro, G. Signorile, G. Fantino, and P. Tavella, "An Efficient and Configurable Preprocessing Algorithm to Improve Stability Analysis," IEEE Trans. Ultrason. Ferroelectr. Freq. Control. **63**(4), 575–581 (2016).
33. P. Defraigne, N. Guyennon, and C. Bruyninx, "GPS Time and Frequency Transfer: PPP and Phase-Only Analysis," Int. J. Navig. Obs. **2008**, 1–7 (2008).
34. D. Xu, E. Cantin, F. Frank, N. Quintin, F. Meynadier, P. Tuckey, A. Amy-Klein, O. Lopez, and P.-E. Pottie, "Two-branch fiber links for international clock networks," IEEE Trans. Instrum. Meas. **68**(6), 2195–2200 (2019).
35. F. Guillou-Camargo, V. Ménoret, E. Cantin, O. Lopez, N. Quintin, E. Camisard, V. Salmon, J.-M. L. Merdy, G. Santarelli, A. Amy-Klein, P.-E. Pottie, B. Desruelle, and C. Chardonnet, "First industrial-grade coherent fiber link for optical frequency standard dissemination," Appl. Opt. **57**(25), 7203–7210 (2018).
36. J. Geršl, P. Delva, and P. Wolf, "Relativistic corrections for time and frequency transfer in optical fibres," Metrologia **52**(4), 552–564 (2015).